

ATOMIC FLUORESCENCE FLAME SPECTROMETRY WITH
A CONTINUOUS WAVE DYE LASER

By

BENJAMIN W. SMITH

A DISSERTATION PRESENTED TO THE GRADUATE COUNCIL
OF THE UNIVERSITY OF FLORIDA
IN PARTIAL FULFILLMENT OF THE REQUIREMENTS FOR THE
DEGREE OF DOCTOR OF PHILOSOPHY

UNIVERSITY OF FLORIDA

1977



ACKNOWLEDGEMENTS

The author wishes to express his sincere appreciation to all of the members of the research group of Dr. J. D. Winefordner for much helpful discussion and assistance. In particular a special expression of gratitude must be made to Drs. David J. Johnson and Nicolò Omenetto for their experimental assistance, theoretical insights and general encouragement.

Dr. James D. Winefordner has been a remarkable research director and deserves much gratitude for making the author's graduate education very rewarding.

TABLE OF CONTENTS

	Page
ACKNOWLEDGEMENTS	ii
ABSTRACT	iv
CHAPTER	
I INTRODUCTION	1
II ATTAINMENT OF SATURATED ATOMIC FLUORESCENCE	5
Theory	5
Population Equalization Approach	7
Line Broadening Approach	12
Experimental Verification of Saturation	16
Experimental Procedure	19
Experimental Concentration Measurement	
Under Conditions of Saturation	28
Experimental Procedure	31
Measurement of $(B_F)_{\max}$	31
Comparison Measurements of n_T	35
Sodium Concentration Profiles for Several Flames	39
Conclusions	44
III FLUORESCENCE SPECTROMETRY OF EXCITED STATE TRANSITIONS	45
Experimental Procedure	46
Operation of the cw Dye Laser	47
Choice of Analytical Lines	51
Analytical Results	54
Discussion	58
IV CONCLUSIONS AND FUTURE WORK	59
REFERENCES	61
BIOGRAPHICAL SKETCH	64

Abstract of Dissertation Presented to the
Graduate Council of the University of Florida
in Partial Fulfillment of the Requirements
for the Degree of Doctor of Philosophy

ATOMIC FLUORESCENCE FLAME SPECTROMETRY WITH
A CONTINUOUS WAVE DYE LASER

By

Benjamin W. Smith

March 1977

Chairman: James D. Winefordner
Major Department: Chemistry

The tunable continuous wave (cw) dye laser has been shown to be capable of producing saturation conditions for sodium in an air - acetylene flame. The experimental evidence indicates that the sodium doublet is a reasonably good approximation of a two-level system. Saturation of the sodium 589.6 nm line was observed at laser spectral irradiances of 10^{13} erg $s^{-1} cm^{-2} nm^{-1}$ and greater. Measurements of the absolute maximum fluorescence radiance under saturation conditions have been used to measure sodium concentration profiles in air - hydrogen and air - acetylene flames with spatial resolution on the order of 0.01 cm. The cw dye laser has also been used as an atomic fluorescence excitation source for analytical purposes and, using resonance fluorescence, limits of detection of $0.0001 \mu g ml^{-1}$ and $0.04 \mu g ml^{-1}$ have been obtained for sodium and barium, respectively. Using nonresonance fluorescence with excited state transitions, limits of detection of

between $0.3 \mu\text{g ml}^{-1}$ and $100 \mu\text{g ml}^{-1}$ were obtained for Cu, Li, Mo, Nd, Rh, Sc, V, and Sr. All transitions were between 550 and 620 nm using rhodamine 6G and sodium fluorescein as laser dyes.

CHAPTER I INTRODUCTION

Soon after the initial analytical development of atomic fluorescence flame spectrometry (AFFS) in 1964 (1), it was realized that the dependence of the atomic fluorescence signal upon the excitation source intensity was a primary limitation to the available fluorescence signal. At that time, only conventional incoherent excitation sources such as hollow cathode lamps and microwave excited electrodeless discharge tubes were available, and these suffered from the disadvantages of low intensity and/or poor stability. Therefore, much of the analytical atomic fluorescence research in the ensuing years was devoted to development of intense, stable sources of excitation. The commercial appearance of the tunable dye laser in the late 1960's has generated much interest in its potential as the ultimate excitation source for atomic fluorescence. The physics of the dye laser has been reviewed by Shank (2) and Webb (3).

The first application of the dye laser to AFFS appeared in 1971 (4) when Fraser and Winefordner used a nitrogen pumped dye laser to excite atomic fluorescence for nine different elements in hydrogen-air and acetylene-air flames. They reported good limits of detection (within 10- or 100-fold of the best reported literature values obtained with conventional

sources) and linear dynamic ranges of about four decades. Their system consisted of a nitrogen laser pumped organic dye laser with peak power of 10 kW, a pulse width of 6 ns, a spectral bandwidth of 1 nm, and a repetition frequency of 1-30 Hz depending upon the dye used. Signal detection and processing were carried out with a 1P28A photomultiplier tube with fast response dynode chain and a boxcar integrator with a 10 ns gate width.

In the same year, Denton and Malmstadt (5) studied the atomic fluorescence of barium excited by a Q-switched ruby laser pumped dye laser and found that an ultrasonic nebulization system was helpful in reducing scatter.

In 1972, Fraser and Winefordner (6) obtained good results for resonance AFS, excited state resonance fluorescence, Stokes direct line fluorescence, anti-Stokes direct line fluorescence and excited state anti-Stokes direct line fluorescence with the same nitrogen laser pumped dye laser system described above. They utilized nonresonance fluorescence to obtain a 10-fold improvement in limits of detection due to decreased scatter. Results such as these point out the versatility of the tunable dye laser as a variable wavelength excitation source. Omenetto et al. (7) studied the laser excited atomic fluorescence of transition elements in the nitrous oxide-acetylene flame in 1973, again using a nitrogen laser pumped dye laser. They stressed the value of nonresonance fluorescence as a means of minimizing spectral interferences and reducing scatter. Omenetto et al. (8) also examined the atomic and ionic fluorescence of the rare earth

elements with a nitrogen pumped dye laser system, observing mainly nonresonance fluorescence transitions; they obtained limits of detection equal or close to the best atomic absorption techniques.

The tunable dye laser has several advantages over conventional line sources: only one source is needed and the source radiation is coherent and thus easily focussed to obtain large power densities. With low duty cycle pulsed laser systems, such as were used by the above authors, the advantage of reduced flame background noise was expected, but not generally realized for various reasons (9). Up to this point in time, no consideration had been given by workers in the field of laser excited AFFS to the possible influence of extremely high source intensities upon the atomic population conditions within the flame. Omenetto et al. (10) and Piepmeier (11) first derived the theory necessary to visualize the influence of saturation of atomic levels by intense laser excitation. Kuhl, Neumann and Kriese have discussed the influence of saturation on flashlamp pumped dye laser excited AFFS (12).

During excitation by conventional low intensity light sources, the fluorescence irradiance is known to be linear with source intensity (13). This relationship holds only up to the point at which the intensity of the source becomes large enough to alter the thermal atomic distribution in the flame. A nearly saturated fluorescing atomic population in a typical analytical flame results in emission signals orders of magnitude larger than the thermally excited emission.

Furthermore, under conditions of saturation, the fluorescence is no longer linearly dependent upon source intensity; it may follow a squareroot dependence or even be independent of source intensity, depending on the type of laser source employed. Also, at saturation the fluorescent emission shows little dependence on changes in collisional quenching (e.g., quantum efficiency) while retaining a linear dependence upon atomic vapor density within the hot gases (assuming the vapor is dilute).

CHAPTER II ATTAINMENT OF SATURATED ATOMIC FLUORESCENCE

The attainment of saturation within an atomic vapor provides a means of measurement of absolute concentrations of atomic species in an analytical flame. In this section will be given a detailed theoretical treatment of steady state saturation by two different approaches, a verification of the effect experimentally and its application to measurements of concentration profiles in several flames of analytical interest.

Theory

There are two distinct approaches available for a theoretical evaluation of the saturation phenomena. The first, and most straightforward, follows the derivation given by Omenetto and Winefordner (14); it is based on the consideration that the absorption coefficient goes to zero at high excitation irradiance because the populations of the levels involved are equalized. In the saturated steady state, the rate of absorption and the rate of emission are equal and no net absorption may occur. This will be referred to as the "population equalization" approach.

A second method for arriving at an expression for fluorescence irradiance at high source intensity is suggested by Killinger et al. (15) in their derivation for laser saturated gas phase molecular fluorescence of OH and by Pantell and Puthoff (16). An extension of their approach to the atomic case leads to the same result as that given by Omenetto and Winefordner. Because the derivation is based upon a consideration of linebroadening as the controlling parameter affecting saturation, this will be called the "broadening" approach.

For either derivation, the following assumptions are made: (i) the atomic system is characterized as an ensemble of atoms having only two energy levels 1 and 2 without multiplet splitting, with equal statistical weights $g_1 = g_2$, separated by the energy difference $E = h\nu_0$, and having populations n_1 and n_2 , with $n_1 + n_2 = n_T$, where n_T is the total density of the atoms; (ii) the atoms are present in thermodynamic equilibrium at low concentration (i.e., selfabsorption is not considered); (iii) the laser radiation does not affect the energy distribution of the gas molecules, the velocity distribution of the atoms, and the temperature T of the system; (iv) polarization effects are neglected; (v) the atomic system is spatially homogeneous with respect to both concentration and temperature; (vi) the radiation density of the source is spatially homogeneous and constant while traversing the system; and finally (vii) steady state conditions have been achieved. It is also necessary to make some assumptions concerning the spectral nature of the laser source with respect to the atomic absorption profile of the atoms within the flame. The situation

is complicated by the fact that the spectral output of the continuous wave (cw) dye laser is not uniform but consists of a series of narrow spectral modes within the narrow spectral output produced by the tuning element within the dye laser cavity. For the laser used in this study, the overall output linewidth is 0.08 nm (FWHM). This linewidth is composed of some 65 spectral modes, each mode having a width of 8×10^{-6} nm with a space between modes of 4×10^{-4} nm. Therefore, over a typical atomic absorption linewidth in the flame of 0.01 nm there are about 25 individual spectral components each about 10^{-5} nm wide. The interaction of each of these modes with the absorption profile causes considerable collisional and Doppler broadening resulting in a more or less continuous absorption over the atomic absorption profile. The assumption is made, then, that the laser acts as a quasi-continuum source, i.e., the overall linewidth of the laser is sufficiently broader than the atomic absorption width in the flame such that the source may be considered to approach a continuum. The experimental results appear to confirm this assumption.

Population Equalization Approach

Based upon simple kinetic considerations (14), the time dependent concentration of the excited state, n_2 , can be represented as

$$\frac{dn_2}{dt} = B_{\rho} v_0 (n_1 - n_2) + k_{12} n_1 - n_2 (A_{12} + k_{21}) \quad (1)$$

where ρ_{ν_0} is the uniform spectral volume energy density at $\nu = \nu_0$ ($\text{erg Hz}^{-1} \text{cm}^{-3}$) of the quasicontinuum laser, B ($\text{erg}^{-1} \text{cm}^3 \text{s}^{-1} \text{Hz}$) is the Einstein coefficient for absorption and stimulated emission ($B_{12} = B_{21} = B$, since $g_1 = g_2$), k_{12} (s^{-1}) is the unimolecular rate constant for thermal excitation, k_{21} (s^{-1}) is the unimolecular rate constant for thermal or non-radiational de-excitation, A_{21} (s^{-1}) is the Einstein transition probability for spontaneous emission and n_1 and n_2 represent the atomic concentrations (cm^{-3}) residing in levels 1 and 2. At the temperatures of typical analytical flames (2000-4000 K) and for typical energy differences of 2 eV or less, k_{12} is negligible with respect to k_{21} ; and since $\tau \equiv (A_{21} + k_{21})^{-1}$, equation 1 reduces to

$$\frac{dn_2}{dt} = B\rho_{\nu_0}n_1 - B\rho_{\nu_0}n_2 - \frac{n_2}{\tau} \quad (2)$$

where τ (s) is the mean radiative lifetime of level 2. Since

$$n_1 = n_T - n_2$$

$$\frac{dn_2}{dt} + \frac{n_2}{\tau} = B\rho_{\nu_0}(n_T - n_2) - B\rho_{\nu_0}n_2$$

or

$$\frac{dn_2}{dt} + \frac{n_2}{\tau} = B\rho_{\nu_0}n_T - 2B\rho_{\nu_0}n_2$$

or

$$\frac{dn_2}{dt} + \frac{n_2}{\tau} (2B\rho_{\nu_0} + 1) = B\rho_{\nu_0}n_T \quad (3)$$

From the theory of radiation

$$B = \frac{c}{h\nu_0} (n_1 - n_2)^{-1} \int_{\text{line}} k(\nu) d\nu \quad (4)$$

where c is the velocity of light (cm s^{-1}) and $k(\nu)$ (cm^{-1}) is the frequency-dependent atomic absorption coefficient of the atomic vapor. The frequency dependent absorption cross-section $\sigma(\nu)$ (cm^2) is related to $k(\nu)$ by (17)

$$\int \sigma(\nu) d\nu = (n_1 - n_2)^{-1} \int_{\text{line}} k(\nu) d\nu \quad (5)$$

which converts equation 4 to

$$B = \frac{c}{h\nu_0} \int_{\text{line}} \sigma(\nu) d\nu \quad (6)$$

Substituting equation 6 into equation 3 gives

$$\frac{dn_2}{dt} + \frac{n_2}{\tau} \left[\frac{2c}{h\nu_0} \rho_{\nu_0} \tau \int_{\text{line}} \sigma(\nu) d\nu + 1 \right] =$$

$$\frac{c}{h\nu_0} \rho_{\nu_0} n_T \int_{\text{line}} \sigma(\nu) d\nu \quad (7)$$

For convenience and simplification let $E_{\nu_0} = \rho_{\nu_0} c$, where E_{ν_0} ($\text{erg s}^{-1} \text{cm}^{-2} \text{Hz}^{-1}$) is the spectral irradiance of the laser. By defining a saturation spectral irradiance parameter $E_{\nu_0}^s$ as (18)

$$\frac{E_{\nu_0}^s}{h\nu_0} \equiv (2\tau \int \sigma(\nu) d\nu)^{-1} \quad (8)$$

equation 7 becomes

$$\frac{dn_2}{dt} + \frac{n_2}{\tau} \left[\frac{E_{\nu_0}}{E_{\nu_0}^s} + 1 \right] = \frac{E_{\nu_0}}{h\nu_0} n_T \int_{\text{line}} \sigma(\nu) d\nu \quad (9)$$

For the case of a dilute atomic vapor, the fluorescence radiance, B_F (erg s⁻¹ cm⁻² sr⁻¹) is given by (13,19)

$$B_F = n_2 h\nu_0 \frac{\ell}{4\pi} (\tau_{sp})^{-1} \quad (10)$$

where ℓ (cm) denotes the depth of the homogeneous fluorescing volume in the direction of observation and τ_{sp} (s) is the radiative lifetime of level 2.

By substituting into equation 9 and rearranging terms

$$\frac{dB_F}{dt} + \frac{B_F}{\tau} \left[1 + \frac{E_{\nu_0}}{E_{\nu_0}^s} \right] = \frac{E_{\nu_0} \ell n_T}{4\pi\tau_{sp}} \int_{\text{line}} \sigma(\nu) d\nu \quad (11)$$

or, if a constant C (Hz sr⁻¹ s⁻¹) is defined as

$$C \equiv \frac{1}{4\pi} \frac{n_T}{\tau_{sp}} \int_{\text{line}} \sigma(\nu) d\nu$$

then

$$\frac{dB_F}{dt} + \frac{B_F}{\tau} \left[1 + \frac{E_{\nu_0}}{E_{\nu_0}^s} \right] = E_{\nu_0} C$$

For a continuous wave dye laser, steady state conditions are assumed, i.e., $dB_F/dt = 0$; thus

$$B_F = C E_{\nu_0} \tau \left[\frac{E_{\nu_0} + E_{\nu_0}^s}{E_{\nu_0}^s} \right]^{-1} \quad (12)$$

In the case of a pulsed laser, steady state conditions may also hold provided that the pulse width of the laser is greater than τ .

Reintroducing the terms involved in the constant C

$$B_F = \frac{\ell}{4\pi} E_{\nu_0} \frac{\tau}{\tau_{sp}} n_T \left[\frac{E_{\nu_0}^s}{E_{\nu_0} + E_{\nu_0}^s} \right] \int_{\text{line}} \sigma(\nu) d\nu \quad (13)$$

Remembering that the transition probability is defined as $A_{21} \equiv (\tau_{sp})^{-1}$ and substituting equation 8

$$B_F = \frac{\ell}{4\pi} E_{\nu_0} A_{21} \frac{h\nu_0}{2 E_{\nu_0}^s} n_T \left[\frac{E_{\nu_0}^s}{E_{\nu_0} + E_{\nu_0}^s} \right] \quad (14)$$

Now, if the source irradiance $E_{\nu_0} \gg E_{\nu_0}^s$ (high irradiance case) saturation has occurred and equation 14 reduces to

$$(B_F)_{\max} = \frac{\ell}{4\pi} A_{21} h\nu_0 \frac{n_T}{2} \quad (15)$$

where $(B_F)_{\max}$ represents the maximal fluorescence radiance obtainable for a given n_T . Thus, an absolute measurement of $(B_F)_{\max}$ yields the product of $n_T A_{21}$, all other parameters being known. The great advantage of determining this product under conditions of saturation is that the measurement is independent of source spectral irradiance, temperature of the atomic system, and quantum efficiency for the transition.

The physical significance of the saturation parameter is easily seen if one lets $E_{\nu_0} = E_{\nu_0}^s$ in equation 14. In this case $B_F = (B_F)_{\max}/2$. Thus, $E_{\nu_0}^s$ represents the source spectral irradiance for which the maximum attainable fluorescence radiance is decreased by a factor of 2.

Furthermore, if $E_{\nu_0} \ll E_{\nu_0}^S$ (low irradiance case) equation 14 becomes

$$B_F = \frac{\ell}{4\pi} \frac{E_{\nu_0}}{E_{\nu_0}^S} A_{21} h\nu_0 \frac{n_T}{2} \quad (16)$$

and since, at low irradiance $n_T \cong n_1$ and by reintroducing the definition of $E_{\nu_0}^S$, remembering equation 5 and the definition of quantum efficiency, $Y_{21} \equiv \tau/\tau_{sp}$

$$B_F = \frac{\ell}{4\pi} Y_{21} E_{\nu_0} \int_{\text{line}} k(\nu) d\nu \quad (17)$$

Equation 16 shows the well-known linear dependence of the fluorescence radiance upon the source spectral irradiance and the quantum efficiency of the transition.

Line Broadening Approach

Equations 15 and 17 may also be obtained by a derivation based upon line broadening under the influence of a high radiation field (laser beam) (15). The same assumptions given above are required. When the source spectral width is greater than the atomic absorption width within the flame, the rate of absorption, R_{abs} (photons s^{-1}) is given by

$$R_{abs} = S \int_{\text{line}} E_{PS\nu} \{1 - \exp[-k(\nu)\ell]\} d\nu =$$

$$S \int_{\text{line}} k(\nu) \ell E_{PS\nu} d\nu \quad (18)$$

where

S = cross-section of exciting beam (cm^2);

$E_{\text{PS}\nu}$ = source spectral photon irradiance at frequency ν ($\text{cm}^{-2} \text{ s}^{-1} \text{ Hz}^{-1}$);

$k(\nu)$ = absorption coefficient at frequency ν (cm^{-1});

l = absorption path length (cm);

and when the expression on the right is evaluated for low optical density, i.e., $k(\nu) l \approx 0.05$, equation 18 can be re-written in terms of n_{T} (cm^{-3}) and the absorption cross section $\sigma(\nu)$ (cm^2) as

$$R_{\text{abs}} = S l n_{\text{T}} \int_{\text{line}} E_{\text{PS}\nu} \sigma(\nu) d\nu \quad (19)$$

The absorption cross-section depends upon the broadening processes and the approach to saturation with high intensity sources, the absorption cross-section being the ratio of the power absorbed per absorbing species to the incident power per unit area, i.e., the effective area per absorber which removes energy from the incident beam.

For the case of pure homogeneous (Lorentzian) line broadening and for continuum excitation

$$\int_{\text{line}} E_{\text{PS}\nu} \sigma(\nu) d\nu = \left(\frac{E_{\text{PS}} \sigma_0}{\delta\nu_s} \right) \left(\frac{1}{1 + S_s} \right) \quad (20)$$

where E_{PS} ($\text{cm}^{-2} \text{ s}^{-1}$) is the integrated source irradiance, σ_0 ($\text{cm}^2 \text{ Hz}$) is the integral of $\sigma(\nu)$ over the line, $\delta\nu_s$ (Hz) is the source spectral width (FWHM) and S_s is defined as

$$S_s = 2\tau\nu_0 \frac{E_{PS}}{\delta\nu_s} = \frac{E_{PS}}{E_{PS}^s} \quad (21)$$

Thus, the rate of absorption is given by

$$R_{abs} = S \ell n_T \frac{E_{PS} \sigma_0}{\delta\nu_s} \left(\frac{1}{1 + S_s} \right) \quad (22)$$

Equation 22 may be rewritten

$$R_{abs} = S \ell n_T \int_{\text{line}} \sigma(\nu) d\nu \frac{E_c}{\delta\nu_s h\nu_0} \left(\frac{1}{1 + S_c} \right) \quad (23)$$

where $E_{PS} = E_c/h\nu_0$ and E_c is the source spectral irradiance in $\text{erg s}^{-1} \text{cm}^{-2}$.

Making use of the previous definition of the saturation irradiance, $E_{\nu_0}^s$ (equation 8), equation 23 becomes

$$R_{abs} = S \ell n_T \frac{h\nu_0}{2E_{\nu_0}^s \tau} \frac{E_c}{h\nu_0 \delta\nu_s} \left(\frac{1}{1 + S_s} \right) \quad (24)$$

or

$$R_{abs} = \frac{S \ell n_T E_c}{2\delta\nu_s \tau} \left(\frac{1}{E_{\nu_0}^s + E_{\nu_0}^s S_s} \right) \quad (25)$$

Now, after substitution of equation 8 into equation 21 and converting E_{PS} to E_c

$$S_s = \frac{E_c}{E_{\nu_0}^s \delta\nu_s}$$

and by substituting into equation 25

$$R_{\text{abs}} = \frac{S \ell n_T E_c}{2 \delta v_s \tau} \left(\frac{1}{E_{\nu_0}^S + (E_c / \delta v_s)} \right)$$

Let

$$E_{\nu_0} = \frac{E_c}{\delta v_s}$$

and

$$R_{\text{abs}} = \frac{S \ell n_T}{2\tau} \left(\frac{E_{\nu_0}}{E_{\nu_0}^S + E_{\nu_0}} \right)$$

Since the rate of fluorescence (photons s^{-1}) is given by (20)

$$R_{f1} = \frac{R_{\text{abs}} Y_{21}}{4\pi}$$

then

$$R_{f1} = \frac{S \ell n_T Y_{21}}{8\pi \tau} \left(\frac{E_{\nu_0}}{E_{\nu_0}^S + E_{\nu_0}} \right)$$

By substituting the definition of $Y_{21} \equiv \tau / \tau_{sp}$, defining the fluorescence radiance per cm^2 and since each photon has an energy of $h\nu_0$

$$B_F = \frac{\ell n_T A_{21} h\nu_0}{8\pi} \left(\frac{E_{\nu_0}}{E_{\nu_0}^S + E_{\nu_0}} \right)$$

Multiplying through by $E_{\nu_0}^S / E_{\nu_0}$

$$B_F = \frac{\ell n_T A_{21} h\nu_0 E_{\nu_0}}{4\pi 2 E_{\nu_0}^S} \left(\frac{E_{\nu_0}^S}{E_{\nu_0}^S + E_{\nu_0}} \right) \quad (26)$$

which is identical to equation 14. Substitution of the limiting cases for high and low irradiances leads to the same results because at low irradiance $n_T = n_1$. Although the above derivation assumes only homogeneous broadening, if the assumption of pure inhomogeneous broadening is made, the same result is obtained (15,16).

Experimental Verification of Saturation

Before discussing the experimental verification of saturation, it is worthwhile to obtain some numerical concept of the laser irradiance required to produce saturation as well as the fluorescence radiance to be expected. The saturation irradiance defined in equation 8 may be rewritten in terms of variables which are more readily accessible by substituting from classical radiation theory (18)

$$\int_{\text{line}} \sigma(\nu) d\nu = (\pi e^2/mc) f_{12} \quad (27)$$

and

$$(\tau_{sp})^{-1} = \frac{8\pi^2 \nu_o^2 e^2}{mc^3} f_{12} \quad (28)$$

where e and m are the charge and mass of the electron and f_{12} is the classical absorption oscillator strength. Therefore

$$E_{\nu_o}^S = \frac{4\pi h \nu_o^3}{c^2} (\frac{\tau_{sp}}{\tau}) = \frac{4\pi h \nu_o^3}{c^2} (Y_{21})^{-1} \quad (29)$$

or, converting frequencies to wavelength and evaluating all

constants,

$$E_{\lambda_0}^s = 7.6 \times 10^{23} \lambda_0^{-5} Y_{21}^{-1} \quad (30)$$

where λ has units of nm, Y_{21} is dimensionless and $E_{\lambda_0}^s$ has units of $\text{erg cm}^{-2} \text{ nm}^{-1} \text{ s}^{-1}$. For the sodium line at 589.6 nm the saturation irradiance is $3.6 \times 10^{11} \text{ erg cm}^{-2} \text{ nm}^{-1} \text{ s}^{-1}$, assuming a quantum efficiency of 0.03 which is both a reasonable estimate and a literature value (21) for an air-acetylene flame very similar in composition to the one used in the following experiments. The shape of the B_F vs. $E_{\lambda_0}^s$ curve may be obtained from equation 14 for a given value of n_T since the transition probability for the sodium doublet is well known (22). Figure 1 presents a log-log plot of this curve for several values of Y_{21} . For a quantum efficiency of 1.0, the saturation irradiance is $1.1 \times 10^{10} \text{ erg s}^{-1} \text{ cm}^{-2} \text{ nm}^{-1}$ which must represent the very minimum source irradiance required to approach saturation. In plotting the curves, n_T is assumed to be 10^{10} cm^{-3} and $l = 100 \text{ } \mu\text{m} = 0.01 \text{ cm}$. In all calculations for sodium (589.6 nm) A_{21} is taken to be $6.28 \times 10^7 \text{ s}^{-1}$ (22).

The cw dye laser used in this study provides a maximum output at 589.6 nm of about 1 W with a spectral width (FWHM) of 0.08 nm. Beyond this, the available spectral irradiance at the flame depends only on the tightness with which the laser beam may be focussed. Because the output is TEM_{00} mode, the focussed beam waist diameter is given by (23)

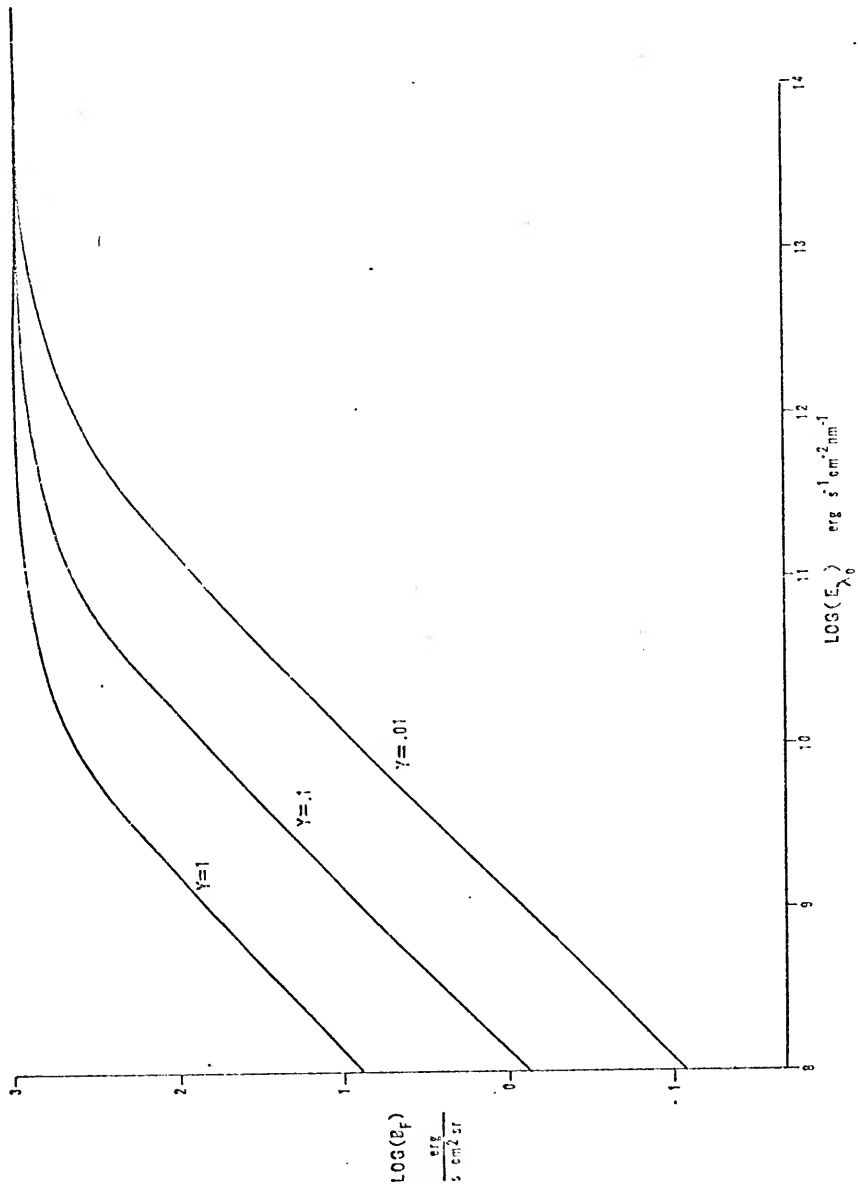


Figure 1. Variation of Atomic Fluorescence with Source Spectral Irradiance for Sodium

$$D_{\text{waist}} = \frac{4 \lambda f}{\pi d} \quad (31)$$

where λ is the wavelength of light passing through the focussing lens, f is the lens focal length, and d is the diameter of the laser beam as it enters the focussing lens. In all cases, a 3.5 in focal length lens has been used ($f = 8.89$ cm), and the beam diameter is approximately 0.5 cm (measured photographically) as it enters the lens; therefore, the waist diameter is 1.3×10^{-3} cm. This corresponds to a focussed spot of 1.3×10^{-6} cm². Therefore, the maximum available spectral irradiance is given by

$$\begin{aligned} E_{\lambda_0} &= \frac{1.0 \text{ W}}{(0.08 \text{ nm})(1.3 \times 10^{-6} \text{ cm}^2)} \\ &= 9.6 \times 10^6 \text{ W cm}^2 \text{ nm}^{-1} \end{aligned}$$

which corresponds to 9.6×10^{13} erg s⁻¹ cm⁻² nm⁻¹ and should thus be nearly sufficient to achieve saturation in sodium if $Y_{21} \geq 0.01$.

Experimental Procedure

A block diagram of the experimental system is shown in Figure 2. The cw dye laser is pumped by all lines of a 4 W argon ion laser. The dye laser output is beam-split to a compact low resolution monochromator for monitoring the laser power continuously via a photomultiplier and an associated DC readout device. This laser energy monitor was calibrated against a certified laser pyrometer at frequent intensity intervals. A summary of the calibration is given in Figure 3

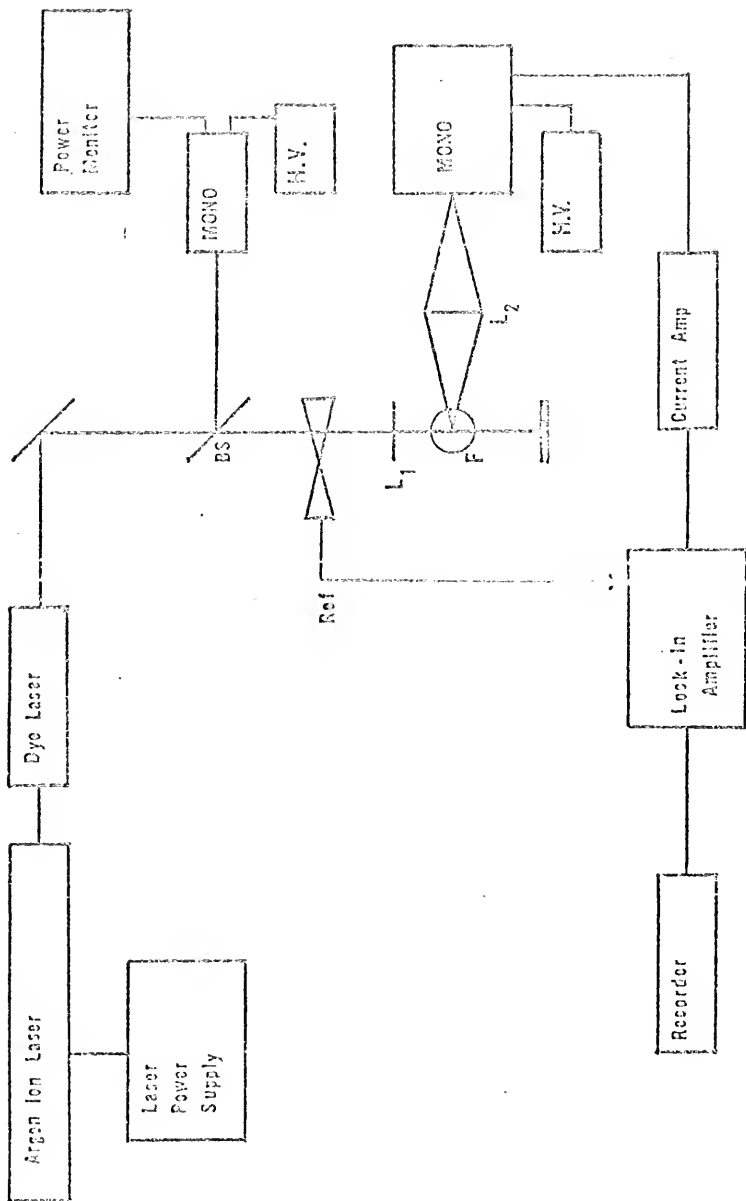


Figure 2. Block Diagram of the Experimental System

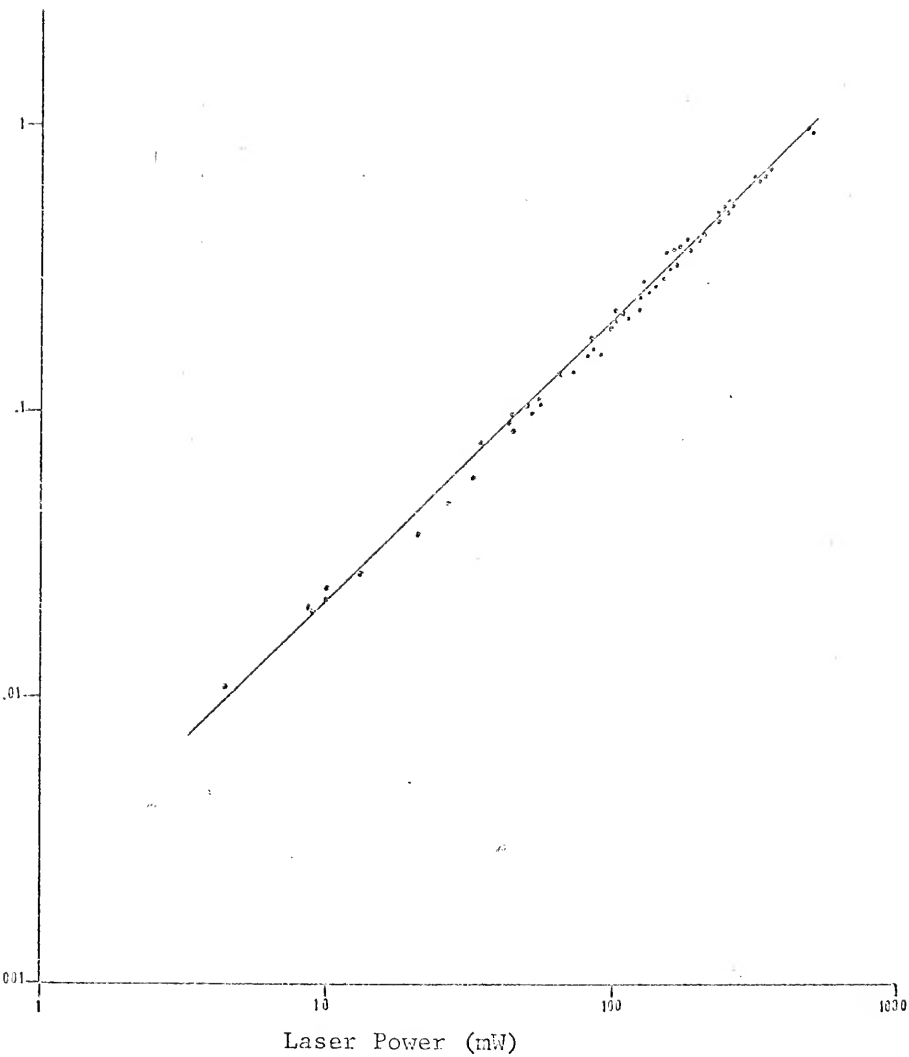


Figure 3. Response of Laser Power Monitor vs. Laser Power

as a plot of relative signal from the beam splitter readout vs. measured laser power in milliwatts. The log-log plot has a slope of 0.97. After passing through the chopper (260 Hz) the beam is steered by two mirrors (not shown) to the height of the burner and focussed by L_1 (focal length 3.5 in) onto the burner center. The collection optics consisted of a single 8 in focal length lens at right angles to the laser beam adjusted to produce a 1:1 image of the focussed beam onto the detection monochromator slit. The detection monochromator was a 0.5 m focal length Czerny-Turner grating spectrometer. The photomultiplier current is converted to a voltage and synchronously detected by a lock-in amplifier which is synchronized with the chopper. The lock-in output is displayed on a strip chart recorder. Table 1 gives the details of all experimental components. By placing neutral density filters between the dye laser and the quartz plate beam splitter, the laser irradiance at the flame may be accurately varied over several decades. When necessary, a tungsten strip lamp was placed at the position of the burner for absolute calibration of the detection spectrometer. The calibration procedure will be discussed later. Flame gases were all standard commercial grades with no filtering. After two-stage regulation at the cylinders the gases were passed through calibrated rotometer flow meters fitted with needle valves and sent to the premix chamber via Tygon tubing. Some fluctuation in the acetylene pressure had been detected in previous studies so a 10 l stainless steel ballast tank was placed in

Table 1
Experimental Components and Manufacturers

Item	Model No.	Source
Argon Ion Laser	552	Control Laser Corp., Orlando, FL
Cw Dye Laser	590	Coherent Radiation, Palo Alto, CA
Tungsten Strip Lamps	EP UV 1068 EP UV 1104	Eppley Laboratory, Inc., Newport, RI
Photomultiplier Tube	1P28A	RCA, Electronics Com- ponents, Harrison, NJ
Photomultiplier Tube	R818	Hamamatsu Corp., Middlesex, NJ
Photomultiplier Housing	180	Princeton Applied Re- search, Princeton, NJ
H. V. Power Supply	244	Keithley Instruments, Cleveland, OH
H. V. Power Supply	EV-42A	Heath Instruments, Benton Harbor, MI
Monochromator	1870	Spex Industries, Metuchen, NJ
Strip Chart Recorder	Servoriter II	Texas Instruments Corp., Houston, TX
Current-to- Voltage Converter	427	Keithley Instruments, Cleveland, OH
Lock-in Amplifier	840	Keithley Instruments, Cleveland, OH
Signal Generator	180	Wavetek, San Diego, CA
Laser Power Meter	210	Coherent Radiation, Palo Alto, CA
Strip Lamp Power Supply	-	Laboratory Constructed, 0 - 50 A, 12 V DC, University of Florida

Table 1 - continued

Item	Model No.	Source
Flow Meters	E29-R-150mm4 E29-4-150mm3	Air Products Corp., Allentown, PA
Burner Nebulizer	303-0110	Perkin-Elmer, Norwalk, CT
Front Surface Mirrors	02-MPQ-001-023	Melles Griot, Irvine, CA

the fuel gas flow line between the supply cylinder and the flowmeters. A two-way valve was provided in the oxidant line to select nitrous oxide or air.

In order to experimentally verify equation 14, it was necessary to obtain values of relative fluorescence vs. laser spectral irradiance over as wide a range of laser intensity as possible. However, with the laser tightly focussed and with a 100 μm slit width to restrict the detection region to the very center of the laser focus waist, it was found that a severe reduction in signal-to-noise ratio occurred at laser irradiances of more than two decades below the maximum. To achieve a reliable indication of the slope at low irradiance it was necessary to remove the laser focussing lens, thereby achieving a spectral irradiance reduction of about five decades while maintaining an adequate signal-to-noise ratio due to the much larger volume of sodium atoms within the excitation region. Measurements were made, then, over two regions of interest: a low irradiance case and a high irradiance case. To establish the integrity of the measuring system, data was taken on the Raleigh scatter resulting from the tightly focussed laser impinging upon a flowing clean air stream. The log-log plot provided a slope of 0.97 (3% low), indicating that the instrumental system performed adequately.

Figure 4 shows the graphical summary of the results for sodium saturation along with a theoretical curve for $Y_{21} = 0.03$ and $n_T = 10^{10} \text{ cm}^{-3}$. To satisfy the requirement of a

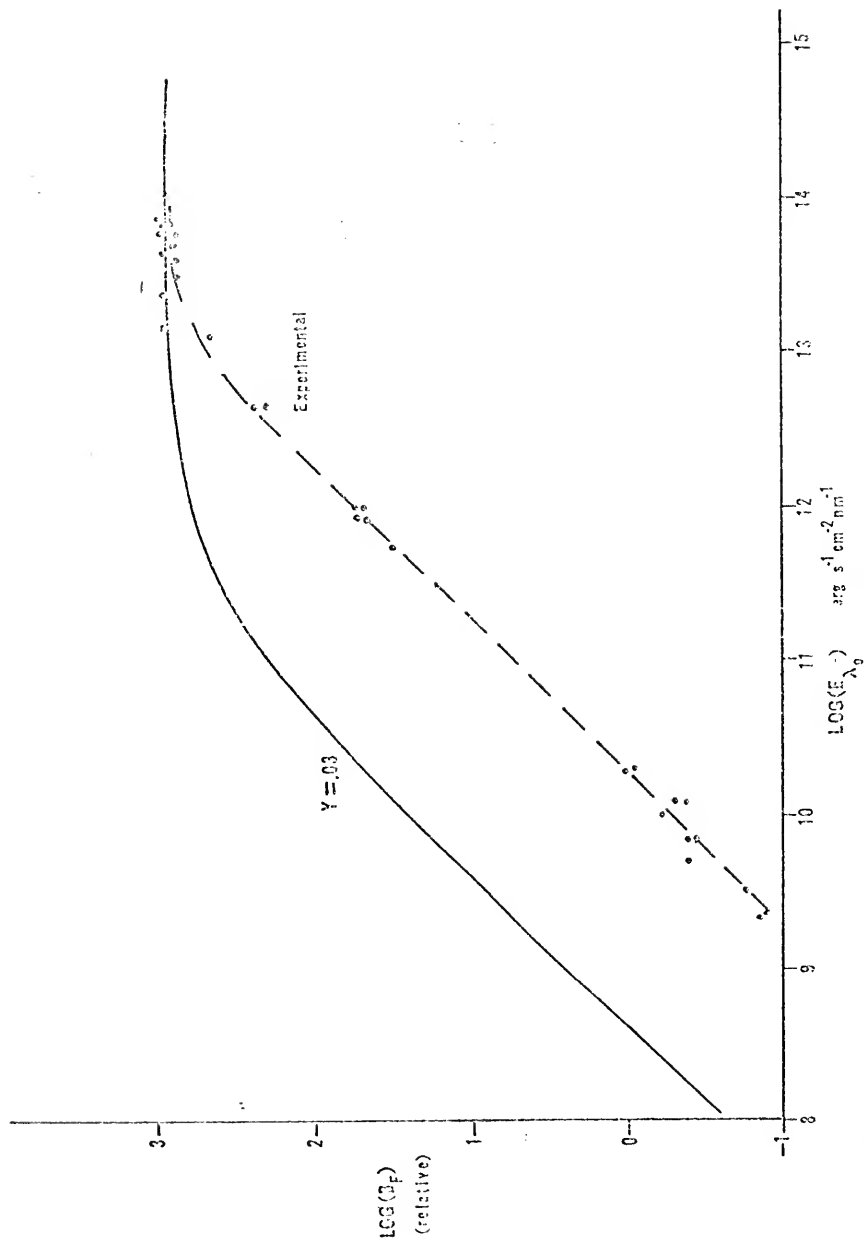


Figure 4. Experimental and Theoretical Curves for the Atomic Fluorescence of Sodium vs. Source Spectral Irradiance

dilute atomic vapor and to minimize any post- or pre-filter effects, all data were taken while aspirating a 1.2 ppm solution of sodium which provided about 10^{10} atoms cm^{-3} in the flame gases. The results shown in Figure 4 were taken on an air-acetylene flame with an argon shield. The ordinate axis for the relative experimental data has been adjusted to coincide with the theoretical curve.

Figure 4 clearly shows the effect of saturation at source spectral irradiances greater than 2×10^{13} $\text{erg s}^{-1} \text{cm}^{-2} \text{nm}^{-1}$. The average of the twelve points taken at the top of the plot is 838 ± 73 (relative units) which gives a saturation irradiance of 8.0×10^{12} $\text{erg s}^{-1} \text{cm}^{-2} \text{nm}^{-1}$. From equation 30 a quantum yield of 1.3×10^{-3} is calculated. The fact that this quantum yield is about an order of magnitude lower than the expected value of 0.03 (21) indicates that the calculated value of saturation irradiance is probably too low. The agreement between theory and experiment is nevertheless satisfying when the uncertainties in the parameters involved are considered and it is remembered that the simple model (14) neglects all line profile effects and the influence of non-quenching collisions. It is likely that efficient interlevel mixing between the upper levels of the sodium doublet results in a larger saturation irradiance than predicted since a fraction of the laser excited sodium atoms in the 16956 cm^{-1} level may lose their absorbed energy by radiative decay via the 16973 cm^{-1} level.

An attempt was also made to measure the effect of satura-

tion on the resonance barium transition at 553.5 nm using fluorescein dye in the laser. However, the peak source spectral irradiance of the dye laser at this wavelength is smaller by a factor of four ($1.2 \times 10^{13} \text{ erg s}^{-1} \text{ cm}^{-2} \text{ nm}^{-1}$) and because the saturation irradiance is proportional to λ^{-5} , the barium saturation irradiance is calculated to be $1.5 \times 10^{12} \text{ erg s}^{-1} \text{ cm}^{-2} \text{ nm}^{-1}$ (for $Y_{21} = 0.01$); therefore the laser was not intense enough to induce a curvature in the plot of source irradiance vs. relative fluorescence. The experimental data with a slope of 0.97 are plotted in Figure 5.

Experimental Concentration Measurement Under Conditions of Saturation

As previously mentioned, equation 15 provides a means of obtaining absolute local species concentrations in a flame by a measurement of the absolute spectral radiance of the fluorescence signal $(B_F)_{\text{max}}$. Substituting the appropriate parameters into equation 15 (see Table 2) gives for sodium (589.6 nm)

$$(B_F)_{\text{max}} = 8.39 \times 10^{-8} n_T \quad (32)$$

where n_T has units of cm^{-3} and $(B_F)_{\text{max}}$ is the maximum radiance under saturation conditions ($\text{erg s}^{-1} \text{ cm}^{-2} \text{ sr}^{-1}$). For the verification of equation 32, the concentration n_T was obtained by two independent methods and compared with the value obtained from a measurement of $(B_F)_{\text{max}}$.

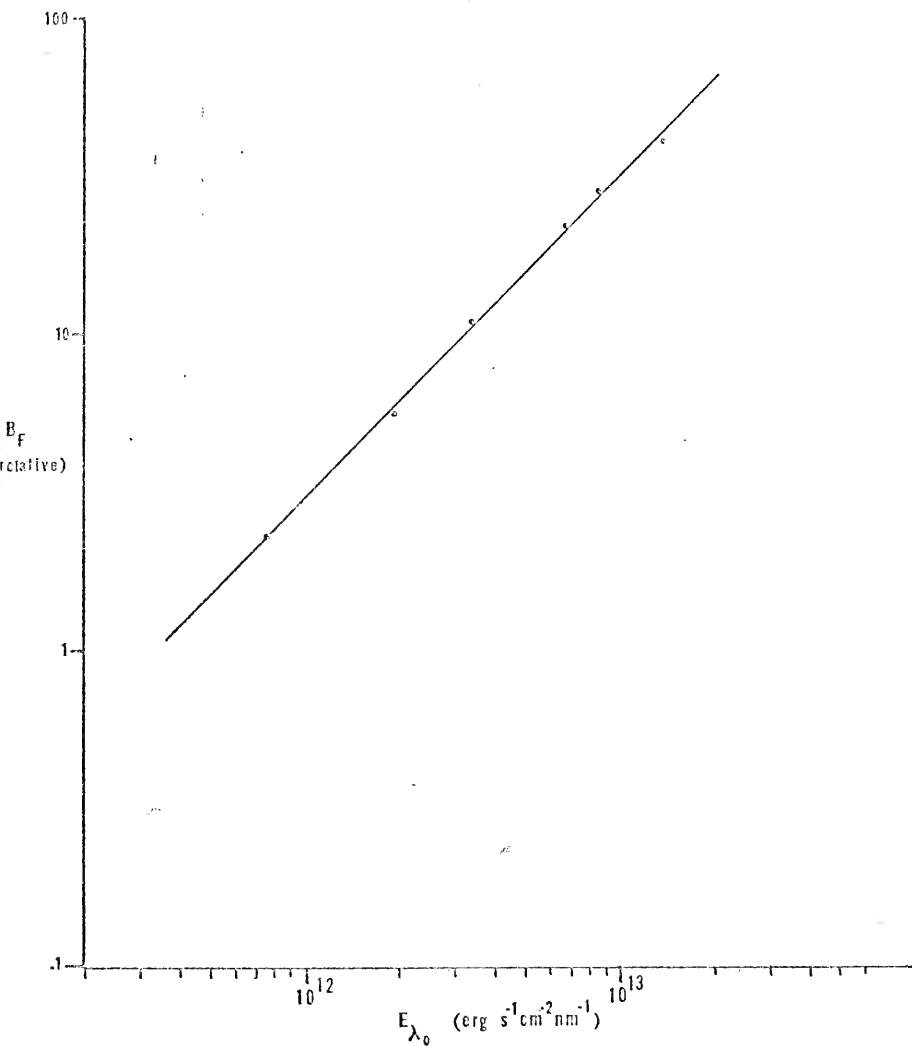


Figure 5. Experimental Variation of Atomic Fluorescence with Source Spectral Irradiance for Barium

Table 2
Spectroscopic and Instrumental Parameters
for Sodium

Wavelength	589.6 nm
Energy of the Transition ($h\nu_0$)	3.36×10^{-12} erg
Transition Probability (A_{21})	0.628×10^8 s ⁻¹
Path Length (l)	0.01 cm
Statistical Weight ($g_1 = g_2$)	2

Experimental Procedure

Measurement of $(B_F)_{\max}$. Because $(B_F)_{\max}$ must be known in absolute radiance units, it was necessary to calibrate the spectrometer detection system in absolute units. This was done by placing a standard NBS-traceable tungsten filament strip lamp at the flame so that the center of the tungsten filament corresponded to the point of minimum beam waist diameter in the focussed laser beam. A calibration factor was then obtained by measuring the photocurrent corresponding to the known spectral radiance of the standard lamp and accounting for the difference in area of the filament and focussed laser beam and the spectrometer bandwidth as follows

$$C' = \frac{i_D}{(B_{\text{lamp}}^O)(\Delta\lambda_m)} \frac{A}{B} \quad (33)$$

where C' ($A \text{ erg}^{-1} \text{ cm}^2 \text{ s sr}$) is the calibration factor, i_D (A) is the detector photocurrent, B_{lamp}^O ($\text{erg s}^{-1} \text{ cm}^{-2} \text{ nm}^{-1} \text{ sr}^{-1}$) is the absolute spectral radiance of the lamp at λ_0 , $\Delta\lambda_m$ (nm) is the spectrometer spectral bandwidth and

$$A = (D_{\text{waist}})(S)$$

and

$$B = (h_m)(S)$$

where A (cm^2) is the area of the focussed laser beam passing into the slit, S (cm) is the spectrometer slit width, B (cm^2) is the area of the slit aperture (fully illuminated by the tungsten filament) and h_m (cm) is the slit height.

The calibration was made with two different lamps (see Table 1) and the results coincided within 3%. The lamps were operated at 35 A according to specifications of the National Bureau of Standards. Remeasurement of the calibration factor on subsequent days (a total of four separate measurements with each lamp) produced a repeatability of about 5%. The values of the terms used in equation 33 are summarized in Table 3. For 589.6 nm the value of C' was 2.0×10^{-12} ($\text{erg}^{-1} \text{ A cm}^2 \text{ s sr}$).

A "standard" air-acetylene premixed flame was used for all measurements of n_T . The burner consisted of a commercially available Perkin-Elmer premixed aspiration chamber fitted with a laboratory constructed, stainless steel capillary burner 1 cm in diameter. The burner head has been described by Haraguchi and Winefordner (24). The capillary burner head was surrounded by a laboratory constructed circular casing through which argon was passed to act as an inert sheath. Table 4 gives the pertinent burner characteristics. A dilute solution of sodium in deionized water was prepared for use in all of the following saturation-related experiments. The sodium concentration was carefully determined by conventional flame emission and found to be 1.2 ppm. The concentration was checked against freshly prepared standards at several times during the course of the experiments and found to be constant.

Aspiration of a 1.2 ppm sodium solution produced 5×10^{-9} A of photocurrent corresponding to a $(B_F)_{\text{max}}$ of 2.5×10^3

Table 3
 Experimental Parameters for the Absolute Calibration
 of the Instrumental System

B_{lamp}° (EP UV 1104, 589.6 nm)	$6.50 \times 10^4 \text{ erg s}^{-1} \text{ cm}^{-2} \text{ nm}^{-1} \text{ sr}^{-1}$
B_{lamp}° (EP UV 1068, 589.6 nm)	$5.78 \times 10^4 \text{ erg s}^{-1} \text{ cm}^{-2} \text{ nm}^{-1} \text{ sr}^{-1}$
D_{waist}	$1.3 \times 10^{-3} \text{ cm}$
h_{m}	0.2 cm
S	0.01 cm
$\Delta\lambda_{\text{m}}$	0.197 nm

Table 4
 Flame and Nebulizer Characteristics
 for the Standard Air-Acetylene Flame

Acetylene Flow ^a	2.60 l min ⁻¹
Air Flow ^a	15.4 l min ⁻¹
Aspiration Rate (ϕ) ^a	8.33 cm ³ min ⁻¹
Aspiration Efficiency (γ) ^a	0.0686
Solution Concentration ^a	1.2 μ g ml ⁻¹
Total Gas Flow Rate (Q) ^a	18 l min ⁻¹
Temperature (T) ^b	2450 K
n_T/n_{293} ^c	1.03
Free Atom Fraction (β) ^d	0.50
Atomization Efficiency (ϵ) ^c	1.0

^aExperimentally measured

^bEstimated

^cFrom reference 25

^dFrom reference 26

erg s⁻¹ cm⁻² sr⁻¹. The laser spectral irradiance for this measurement was 4.6×10^{13} erg s⁻¹ cm⁻² nm⁻¹ which, referring to Figure 4, is sufficient to establish saturation. Then, from equation 32, $n_T = 3.0 \times 10^{10}$ cm⁻³. The possible influence of polarization of the laser beam on these measurements was investigated and found negligible. Mathematically, the calculation of $(B_F)_{\max}$ may be expressed as

$$(B_F)_{\max} = \frac{5 \times 10^{-9} \text{ A}}{C} \text{ erg s}^{-1} \text{ cm}^{-2} \text{ sr}^{-1}$$

Comparison Measurements of n_T . Independent measurements of n_T were carried out by two methods. First, the concentration of sodium atoms in the flame may be calculated from a knowledge of the flame characteristics following the procedure given by Winefordner et al. (25,27). This requires a knowledge of the total gas flow rate Q (cm³ s⁻¹), the solution aspiration rate, ϕ , (cm³ min⁻¹), the aspiration efficiency, γ , (no units), the flame temperature, T , (K), the free atom fraction, β , (no units), the atomization efficiency, ϵ , (no units), and the concentration of the solution, C_m , (moles l⁻¹). The flame concentration is then given by

$$n_T = \frac{C_m \phi n_{298} \epsilon \beta \gamma}{3.3 \times 10^{-22} Q T n_t} \quad (34)$$

where n_{298} and n_t represent the number of moles of combustion products present at room temperature and at flame temperature, respectively. The calculation may be considered only as

approximate because several of the parameters (β , ϵ , T) must be estimated or obtained from literature sources. Nevertheless, it is useful to make the calculation and for the flame specified in Table 4, $n_T = 6.1 \times 10^{11} \text{ cm}^{-3}$.

An experimental value of n_T may be obtained by a measurement of the total absorption of the flame against a background continuum source at the wavelength of the transition of interest. The procedure has been outlined by Zeegers and Winefordner (28). The experimental setup is as previously described except that a 600 W quartz iodine lamp is placed behind the flame, collimated, chopped and focussed at the flame center. By scanning the spectrometer (with 0.03 nm bandpass) across the sodium absorption line at either 589.6 nm or 558.9 nm, it is possible to obtain a value of the total absorption, α , from which the flame concentration n_T may be calculated via

$$n_T = \frac{\pi m c^2}{\pi e^2 \lambda^2 f \ell} \frac{Z}{g_0} \Delta \lambda_m \alpha \quad (35)$$

where m (g) is the mass of the electron, c (cm s^{-1}) is the speed of light, e ($\text{cm}^{3/2} \text{ g}^{1/2} \text{ s}^{-1}$) is the charge of the electron, λ (cm) is the peak wavelength of the absorption transition, f (no units) is the oscillator strength, ℓ (cm) is the path length through the flame, Z (no units) is the partition function for sodium, $\Delta \lambda_m$ (cm) is the bandwidth of the spectrometer, and α (no units) is the measured fraction of the incident intensity absorbed. For the 589.6 nm sodium transition $f = 0.655$, $g_0 = 2$, and $Z = 2$. Because $\ell = 1$ cm, equation 35 re-

duces to

$$n_T = 1.5 \times 10^{12} \alpha$$

and while aspirating a 1.2 ppm sodium solution α was found to be 0.017. The total absorption method gives, then, a flame concentration of $n_T = 2.6 \times 10^{10} \text{ cm}^{-3}$.

Table 5 summarizes the results for the three determinations of n_T . The value obtained from equation 34 can be taken only as a rough estimate, and so the discrepancy between it and the saturation value is not disappointing. In particular, the free atom fraction, β , is in error by as much as 25% (26) and the parameters which depend upon the gas flow rates (Q , ϕ) are only known to within 10% (the reproducibility of the flowmeters). Also, the flame temperature, T , has been taken from the literature (26) and is, at best, accurate to ± 50 K for the particular flame used in this study. These four variables introduce a total uncertainty of about $\pm 60\%$. The value of n_T obtained by the total absorption measurement should be much more accurate. Since all the variables in equation 35 are well-known, the primary source of error in the total absorption result arises from the measurement of α . The signal-to-noise ratio at a sodium concentration of 1.2 ppm was insufficient for an accurate measurement of total absorption, and it was necessary to measure α at concentrations of 10 ppm and higher and perform a graphical extrapolation to the lower concentration. Pronounced curvature was present in the growth curve above 100 ppm, and so the extrapolation was carried out on the linear portion of the curve from 10 to 100 ppm. The plot obtained is quite linear (slope = 0.633, correlation coef-

Table 5
Results of the Three Determinations of n_T

Saturation ^a	$3.0 \times 10^{10} \text{ cm}^{-3}$
Total Absorption ^b	$2.6 \times 10^{10} \text{ cm}^{-3}$
Calculated ^c	$6.1 \times 10^{11} \text{ cm}^{-3}$

^aFrom equation 32

^bFrom equation 35

^cFrom equation 34

efficient = 0.997), and the good correlation coefficient indicated that any error present probably amounts to less than 5%. The 13% discrepancy between n_T obtained via saturation and the total absorption technique is then quite acceptable. The largest source of error present in the saturation determination is the calculation of the laser beam focus waist which is necessary in the calibration procedure. Equation 31 is theoretical and assumes a perfect optical component with no aberrations and a beam which is perfectly coherent. Because neither of these assumptions is valid, there is a possible error which would cause the beam waist to be larger than calculated. This would increase the calibration factor, C , (equation 33) leading to a smaller value of n_T in the saturation determination. Also, a larger beam waist would affect the data shown in Figure 4 because the experimental values of E_{λ_0} would be reduced, causing the experimental data to be shifted to the left, i.e., a larger beam waist results in a lower spectral irradiance.

Sodium Concentration Profiles for Several Flames

The use of laser saturation for the measurement of sodium concentration profiles in flames has the distinct advantage over more conventional techniques (such as total absorption or absolute emission) of being a truly local technique. While line-of-sight methods require an assumption of geometric symmetry within the flame gases and probe techniques tend to disturb the point of measurement, the tightly focussed laser

beam acts as a very high spatial resolution remote probe. This superiority has been applied to two different flames in order to evaluate its suitability as a local species probe.

The experimental setup is identical to that previously described (Figure 1) except that the burner is mounted on a two-dimensional translation stage enabling positioning in the horizontal and vertical axis to within 0.05 cm. Profiles were obtained by measuring the maximum fluorescence $(B_F)_{\max}$ at various points throughout the flames. Table 6 lists pertinent details of the flames studied. The hydrogen-entrained air flame was chosen because it possesses a very cool inner zone and provides an interesting horizontal profile. The air-acetylene flame was studied because of its popularity as an analytical flame.

Figure 6 indicates the horizontal sodium concentration profile in a hydrogen-entrained air flame at heights of 3.4 cm and 4.4 cm above the burner top. Horizontal profiles were measured across the center of the flame. The aspirated solution concentration is 1.2 ppm. Figure 6 clearly shows that the sodium profile is asymmetric and contains a concentration depression of about 0.3 cm width at the flame center. The concentration is reduced at the higher profile which correlates qualitatively with the vertical profile results in air-acetylene.

Figure 7 shows a vertical sodium concentration profile for the air-acetylene flame. It is taken with the laser focussed at the flame center for an aspirated solution concentra-

Table 6
 Flame and Burner Parameters for Flames Used
 in the Profile Studies

Air/Acetylene Flame

Air Flow	9.5 l min^{-1}
Acetylene Flow	1.6 l min^{-1}
Solution Concentration	$1.2 \text{ } \mu\text{g ml}^{-1}$

Hydrogen/Entrained Air Flame

Air Flow	(entrained)
Hydrogen Flow	7.7 l min^{-1}
Argon Flow	6.3 l min^{-1}
Solution Concentration	$1.2 \text{ } \mu\text{g ml}^{-1}$

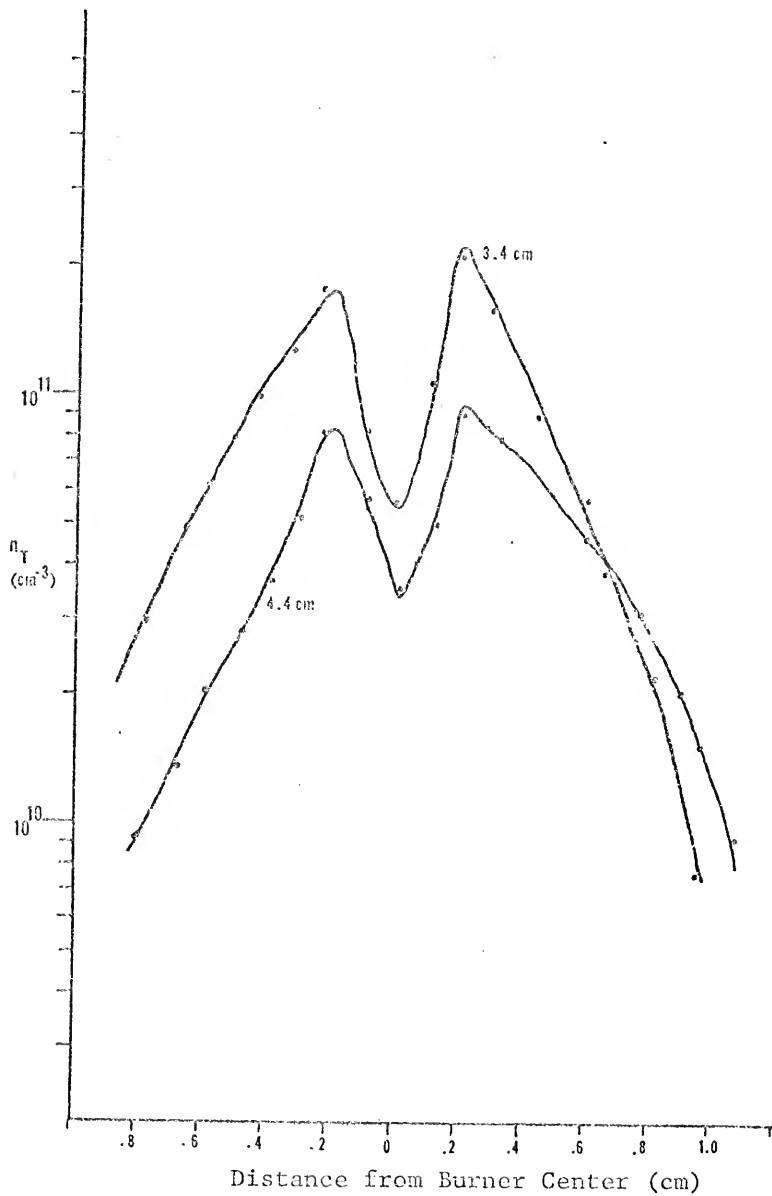


Figure 6. Horizontal Sodium Concentration Profiles in a Hydrogen - Air Flame at 3.4 and 4.4 cm Height above the Burner Tip

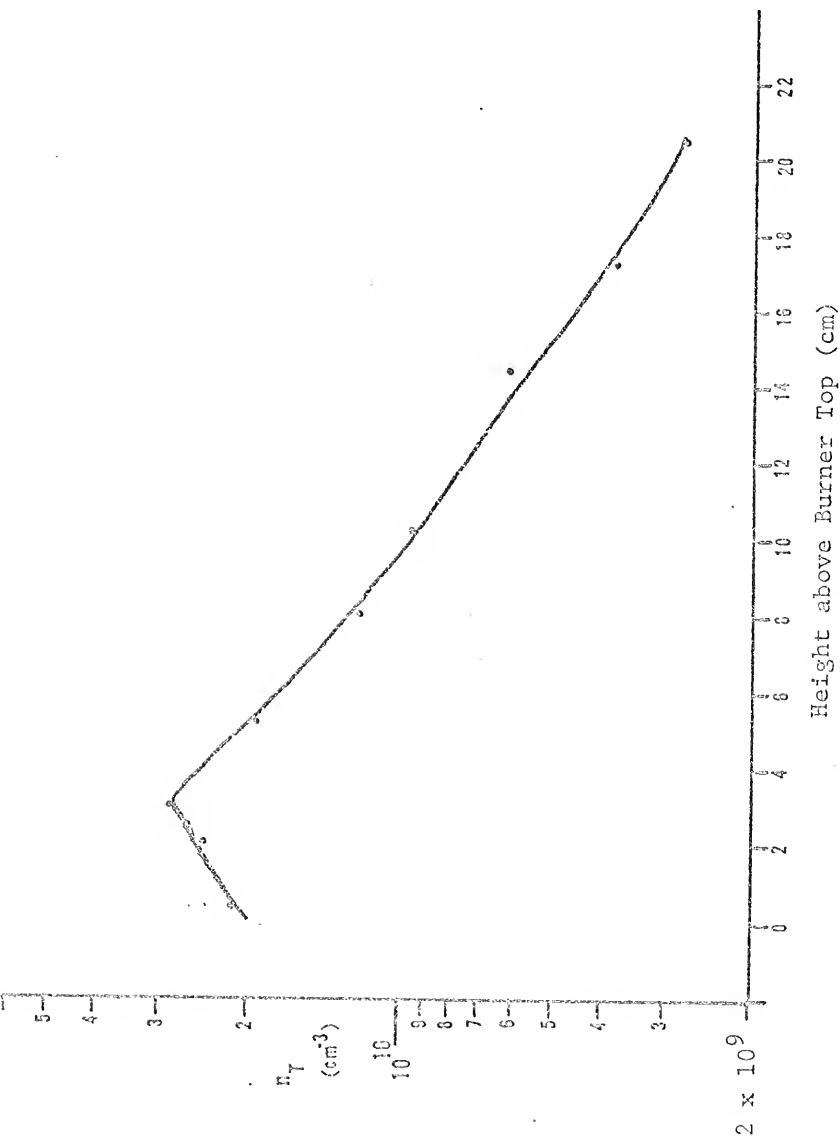


Figure 7. Vertical Sodium Concentration Profile in an Acetylene-Air Flame at the Flame Center

tion of 1.2 ppm. There is a clear maximum in sodium concentration about 0.3 cm above the burner tip.

Conclusions

It has been shown that saturation of sodium atoms does occur in flames under conditions of intense laser excitation. Furthermore, the two-level steady state theory derived for the process has been found to agree well with experiment. The assumption that the 589.6 nm sodium transition acts as a simple two-level system is certainly only approximate because the doublet mixing cross-section is known to be quite large ($\sim 10^{-15} - 10^{-14} \text{ cm}^2$) (29). This probably accounts for the fact that saturation was not achieved at as low of a source spectral irradiance as was predicted. The potential of saturated atomic fluorescence as a probe of atomic specie concentration has been experimentally verified; and, where saturation can be achieved and the assumptions of a nondegenerate two-level atomic system met, it should offer a very useful diagnostic technique for the study of combustion.

CHAPTER III FLUORESCENCE SPECTROMETRY OF EXCITED STATE TRANSITIONS

Analytically, the cw dye laser fluorescence spectrometry system is considerably different than the low duty cycle pulsed laser systems used previously by other workers (4,8,30, 31). Practically, it is a less complicated system to work with because the laser intensity is easily and accurately measurable, and the beam is convenient to align and focus. Because it is a cw source, it may be conveniently chopped, and conventional lock-in detection may be used. At present, the cw dye laser has the decided disadvantage of very limited wavelength tunability. Because the majority of analytically useful atomic fluorescence transitions occur in the blue to ultraviolet region, this limited tunability in the visible region (approximately 520 - 700 nm) is a distinct restriction. Nevertheless, there are a number of useful atomic transitions present in the visible region that have not been previously applied for analytical purposes which may be studied to determine the suitability of the cw dye laser as an atomic fluorescence source. A recent report (32) of a detection limit of 100 atoms cm^{-3} for sodium in a quartz vapor cell indicates the potential of the cw dye laser as an excitation source for analytical atomic fluorescence.

Experimental Procedure

The experimental setup is the same as that shown in Figure 1 with the exception that the single optical lens in the fluorescence collection path was replaced with a collimating lens followed by a dove prism (which rotated the optical image by 90°) and another lens to focus the pencil of fluorescence onto the slit. The use of the dove prism effected an increase of almost two orders of magnitude in the signal-to-noise ratio by allowing efficient collection of the entire pencil of fluorescence generated by the focussed laser beam passing through the flame. In this case, the optimum slit width was a compromise between allowing the full width of this pencil to enter the spectrometer and maintaining a sufficiently narrow spectral bandwidth to minimize flame background noise. For the analytical studies, a red-sensitive photomultiplier tube (Hamamatsu R818) was substituted for the 1P28A photomultiplier tube used previously. As before, Table 1 lists pertinent instrumental details.

Standard stock solutions were prepared from reagent grade chemicals according to the tables given by Smith and Parsons (33). Necessary dilutions were prepared as required at the time measurements were being taken. In all cases, de-ionized water served as the blank. For resonance transitions, it was necessary to synchronously scan the dye laser and the detection monochromator across the atomic line. This was accomplished by preparing calibration curves for each laser dye

(wavelength micrometer reading vs. wavelength) and then driving the wavelength micrometer on the laser with an AC synchronous motor at 1/8 RPM. This provided a scan rate of about 0.01 nm s^{-1} . The stepping motor drive on the detection spectrometer was then driven at the same rate to achieve synchronous scanning. Because the birefringent tuning element in the dye laser cavity was not perfectly linear with wavelength, the scan rate varied from 0.009 to 0.012 nm s^{-1} depending upon the spectral region of the dye being used. The detection monochromator was adjusted to the proper scan rate by driving its stepping motor externally with a precision signal generator of the proper frequency. In general, it was not possible to scan synchronously over a wavelength range of more than 5 nm unless great care was used in matching the rate of the detection monochromator with the rate of the dye laser. Calibration graphs for rhodamine 6G and sodium fluorescein are shown in Figure 8.

For nonresonance transitions, the detection spectrometer was tuned to the fluorescence wavelength of interest by hand and peaked on the background atomic emission signal from the flame. Then, with the detection spectrometer fixed on wavelength, the laser was scanned across the region containing the excitation wavelength while recording the lock-in signal originating from the fluorescence wavelength.

Operation of the cw dye laser

Figure 9 shows a schematic representation of the cw dye

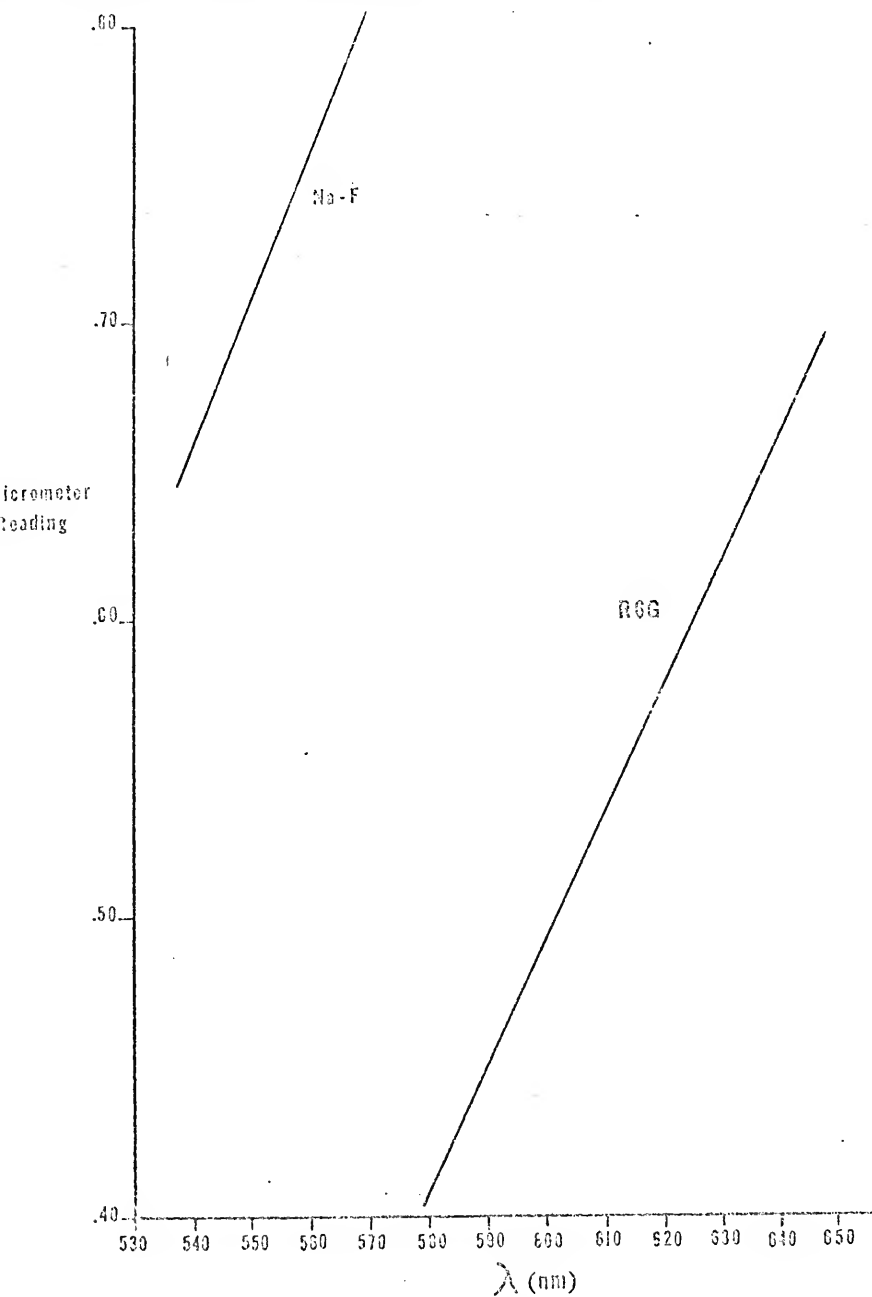


Figure 8. Calibration Graphs for the cw Dye Laser for Rhodamine 6G (R6G) and Sodium Fluorescein (Na-F)

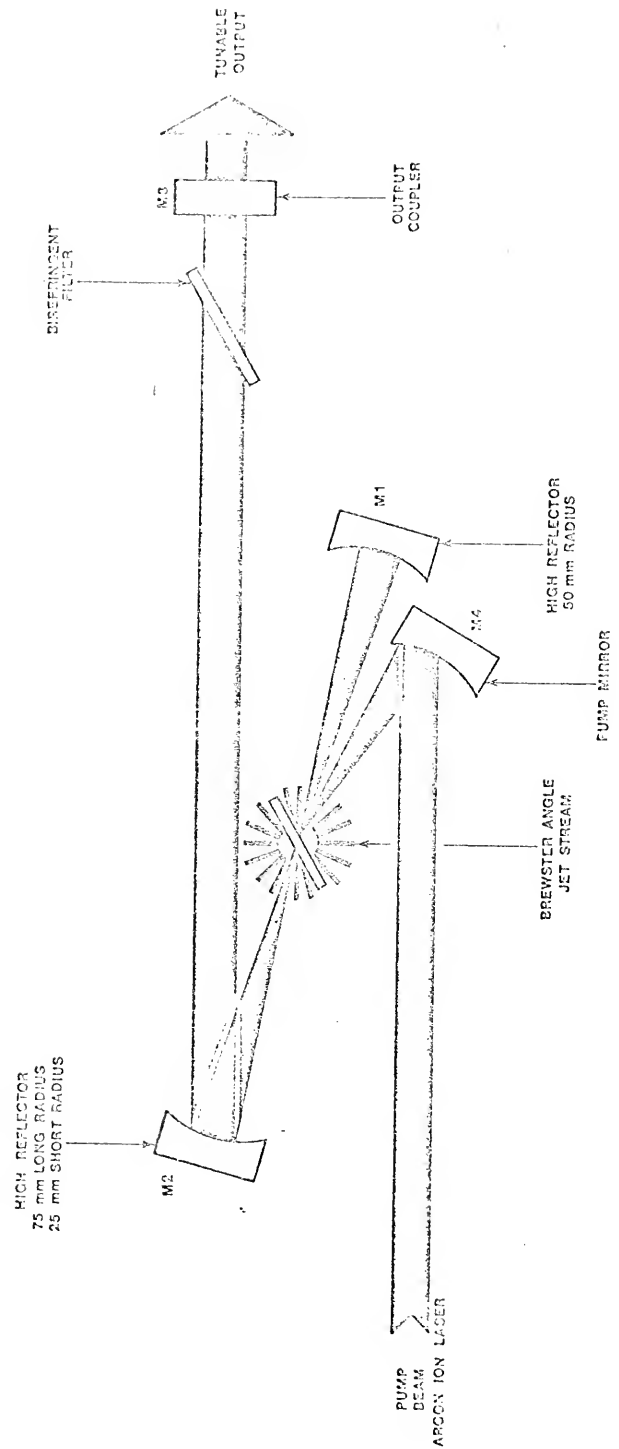


Figure 9 Model 590 Jet Stream Dye Laser
Optical Schematic

laser used in this study. The design is a three mirror, non-collinearly pumped, astigmatically compensated cavity. Pump light from a cw argon ion laser (ca. 4 W, all lines) is focussed onto the dye stream by a pump mirror M4. The dye stream consists of a high viscosity solvent (ethylene glycol) with an organic dye solution at a concentration of 10^{-4} to 10^{-3} M. The dye is water cooled to increase its viscosity and improve jet stream stability. Mirrors M1 and M2 are 5 cm and 7.5 cm focal length high reflectors, respectively. Mirror M3, the output mirror, is flat. Wavelength tunability is achieved by a birefringent filter tuning element consisting of three flat and parallel crystalline quartz plates placed inside the dye laser cavity at Brewster's angle. The plates form a birefringent filter which has low loss for linearly polarized light at a particular wavelength. The plates are oriented so that the optical axis of each crystal is in the plane of the face and the axes of all the crystals are parallel to each other. They function as full-wave plates; as the plates are rotated about a surface normal, the low loss wavelength changes because the extraordinary index of refraction changes. When properly aligned, the dye laser operates at an efficiency (dye laser output/pump laser input) approaching 0.2. In this study, two dyes were used: (i) rhodamine 6G was used for wavelengths between 570 nm and 650 nm; (ii) sodium fluorescein was used between 535 nm and 580 nm. Sodium fluorescein required the addition of COT (cyclooctatetraene) to achieve lasing action (1 - 2 ml ℓ^{-1} of dye solution). The peak output power for each dye was 1.1 and 0.2 W, respectively.

Choice of Analytical Lines

For excited state fluorescence where the absorption transition originates from some state above the ground level, the important spectroscopic parameters for use in choosing the best transition for analysis are the relative atomic population in the excited level and the transition probability (A_{21}) for the fluorescence transition. In choosing the transitions for use in this study, the primary source of data was the NBS tables of transition probabilities compiled by Corliss and Bozman (34). Tables of the relative populations of excited atomic levels were tabulated according to Parsons et al. (35). Absorption transitions for each of the seventy elements included in reference 34 were examined over the wavelength range available with the dye laser (535 - 650 nm) and, in general, any lower level containing 0.1% or more of the element's total atom distribution at 2500 K was considered. In most cases, this required that transitions originating above about $15,000 \text{ cm}^{-1}$ be rejected. Fluorescence transitions throughout the visible and ultraviolet regions (200 - 700 nm) were then examined and those originating from the same upper levels terminated by the suitable absorption transitions, with transition probabilities larger than about 10^7 s^{-1} , were listed for possible experimental consideration. Table 7 lists the elements ultimately studied along with the pertinent spectroscopic data. In some cases (most notably barium), it was possible to choose among several possible combinations of

Element	Lower Level ^a cm ⁻¹	Upper Level ^a cm ⁻¹	$gA \times 10^8$ ^a s ⁻¹	% Population ^b in Lower Level at 2500 K	Wavelength ^a nm
Ba	9216	25957	1.5	2.3	597.17
Ba	9034	25704	1.4	1.5	599.71
Ba	9034	25642	1.4	1.5	601.95
Ba	9216	25704	3.1	2.3	606.31
Ba	9597	25957	5.2	2.6	611.08
Ba	9597	25980	4.0	2.6	649.88
Ba	0	18060	2.0	92.6	553.55
La	4122	21384	0.79	8.0	579.13
La	1053	17910	0.11	28.0	593.06
Na	0	16973	1.8	100	589.00
Na	0	16956	0.90	100	589.59
Mo	0	28924	0.31	99.4	345.64
Mo	11859	28924	0.14	0.11	585.83
V	553	26172	2.4	23	390.23
V	8716	25131	1.3	0.4	609.02
Rh	12723	29431	0.12	0.04	598.30
Rh	0	29431	3.1	60	339.68
Nd	0	17787	0.67	-	562.05
Sc	11610	29190	3.7	0.11	568.68
Sc	11677	29190	0.59	0.13	570.86

Table 7 - continued

Element	Lower Level ^a cm ⁻¹	Upper Level ^a cm ⁻¹	$gA \times 10^8$ ^a s ⁻¹	% Population ^b in Lower Level at 2500 K	Wavelength ^a nm
Sr	18319	36382	2.0	0.02	553.48
Sr	18219	36382	3.4	0.01	550.42
Cu	0	30535	0.13	99.5	327.40
Cu	13245	30535	0.054	0.1	578.21

^aData taken from reference 34

^bData taken from reference 35

absorption transition with fluorescence transition. In the case of barium, excitation at any of the first six wavelengths given in Table 7 resulted in fluorescence at the other five. The close spacing between the upper levels ($\Delta E \approx 300 \text{ cm}^{-1}$) clearly results in very efficient interlevel mixing.

Analytical Results

Limits of detection (LOD) were obtained for eleven elements by atomic fluorescence with the cw dye laser. In most cases, the determination of the LOD was performed as the last step in the measurement of the analytical calibration curve. Signal-to-noise ratios were obtained at the lowest easily measured concentrations (typically about an order of magnitude above the limit of detection) as the average of four to six measurements of an analyte solution against a deionized water blank. The signal-to-noise ratio at this concentration was then extrapolated to a signal-to-noise ratio of two at the limit of detection. Table 8 lists the LOD's, flames, and the excitation and fluorescence lines used for the eleven elements. Also listed are the best reported literature values of the LOD for these elements obtained by atomic fluorescence and atomic absorption flame spectrometry (AAFS) (26). Where it was practical, analytical calibration curves were obtained at solution concentrations up to $1000 \mu\text{g ml}^{-1}$. Figure 10 shows these plots for barium, sodium, vanadium, neodymium, and lithium. The growth curves are linear with slopes close to

Table 8

Analytical Results and Spectroscopic Data for the Elements
for Analytical Use

Element	λ excite	λ fluor	Flame ^a	L.O.D. ^b		L.O.D. ^c Conventional AAFS	L.O.D. ^c AAFS
	nm	nm		$\mu\text{g ml}^{-1}$	$\mu\text{g ml}^{-1}$		
Barium	611.1	606.3	N ₂ O/A	0.5	-	-	0.22
Barium	553.7	553.7	N ₂ O/A	0.04	-	-	0.22
Copper	578.2	327.4	N ₂ O/A	100	0.005	0.005	0.001
Lithium	610.3	610.3	Air/A	0.5	-	-	0.0003
Molybdenum	585.8	345.6	N ₂ O/A	14	0.3	0.3	0.03
Neodymium	562.0	562.0	N ₂ O/A	2	2	2	0.6
Rhodium	598.3	339.7	N ₂ O/A	0.3	0.15	0.15	0.004
Scandium	570.8	568.7	N ₂ O/A	50	0.01	0.01	0.02
Sodium	589.5	589.5	Air/A	0.0001	0.001	0.001	0.001
Uranium	591.5	591.5	N ₂ O/A	500	-	-	12
Vanadium	609.0	609.0	N ₂ O/A	0.3	0.07	0.07	0.02
Strontium	553.5	550.4	Air/A	0.1	0.01	0.01	0.002

^aN₂O/A = nitrous oxide - acetylene flame; Air/A = air - acetylene flame.

^bL.O.D. defined for signal-to-noise ratio = 2.

^cFrom reference 26

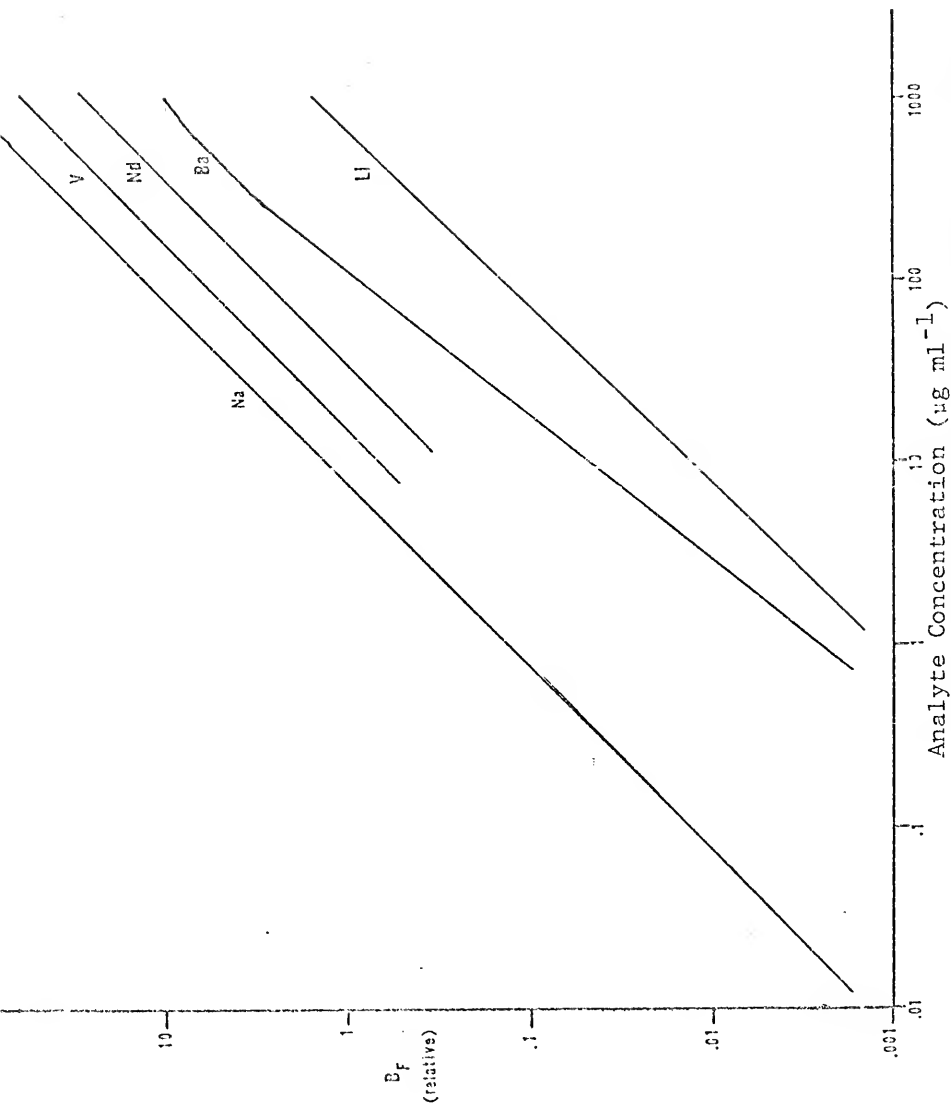


Figure 10. Analytical Curves for Sodium, Vanadium, Neodymium, Barium and Lithium.

unity. In the case of sodium, the linear dynamic range of the analytical curve was observed to be extended at high laser irradiance. At low laser irradiance (unfocussed) the sodium analytical curve showed negative curvature at sodium solution concentrations above $500 \mu\text{g ml}^{-1}$.

Referring to Table 8, the LOD's are found to be better than previous AAFS or conventional AAFS results for sodium and barium where the best resonance line was within the range of the dye laser. For the other elements, the LOD's are inferior to previous AAFS or conventional AAFS results although in some cases (Nd, Rh, V) only slightly so. This is not surprising when one considers the disadvantage of using excited state levels with low populations and the generally poorer transition probabilities of the lines used.

For most of the elements, the nitrous oxide - acetylene flame was necessary to achieve both sufficient excited level populations and greater atomization. For all cases using this flame, the limiting source of noise proved to be flame instability related either to scatter of the laser beam from random particle presence in the flame (in the case of resonance transitions) or to fluctuations in the flame background continuum or band emission (in the case of nonresonance transitions). In order to achieve reproducibility, it was necessary to clean the capillary burner head frequently and to adjust carefully the gas flow system for optimum signal-to-noise ratio.

Discussion

If the cw dye laser were tunable to the best atomic line for an element, it should be capable of producing limits of detection at least one or two orders of magnitude better than conventional atomic fluorescence sources. This is due primarily to the increase in available spectral irradiance achieved with the dye laser. The usefulness of the cw dye laser is enhanced by the ability to select unusual atomic or molecular transitions for analytical use. It appears that unless much larger argon ion laser pumps are used, the available power in the blue region of the spectrum will be too low to achieve full saturation for most elements. However, it is important to emphasize that once saturation is achieved it is disadvantageous to further increase the source intensity since the fluorescence will remain constant while scatter will continue to increase. At present, then, the analytical utility of the cw dye laser is limited primarily by its lack of tunability throughout the ultraviolet and blue spectral regions where the more useful atomic fluorescence transitions occur.

CHAPTER IV CONCLUSIONS AND FUTURE WORK

The tunable cw dye laser has been shown to be capable of producing saturation conditions for sodium and to be a suitable excitation source for analytical atomic fluorescence flame spectrometry. If the tunable wavelength region of the cw dye laser is extended, either by frequency doubling or by use of new dyes or shorter wavelength pump lasers, it should have considerable usefulness as a versatile atomic fluorescence excitation source. At the present level of technology, however, there is still much fluorescence research for which this laser may be advantageously used. When saturation is attained, a measurement of the saturation spectral irradiance, $E_{\lambda_0}^S$, offers a means of determining the quantum efficiency (equation 30). Because saturation can be achieved for sodium it should be possible to make accurate measurements of the sodium quantum efficiency under a variety of flame conditions. Analytically, the discrete spectral nature and tunability of the cw dye laser makes it an ideal source for nondispersive atomic fluorescence. An experimental system using a filter for wavelength selection, a photomultiplier in close proximity to the flame, multipass optics and beam expansion should show considerable improvement in limits of detection for the ele-

ments studied in this work. The cw dye laser should also prove valuable when used with a nonflame atomization cell, such as a carbon rod, because of the reduced background and the ease with which it can be focussed and aligned. The use of intercavity etalons for the selection of a single mode of the dye laser output offers the possibility of investigating the effects of a high intensity narrow line source on atomic fluorescence. As a source for molecular fluorescence, the cw dye laser should prove useful for examining the fine structure of several species which may be present in flames, in particular SrOH and BaO.

REFERENCES

1. J. D. Winefordner and T. J. Vickers, Anal. Chem., 36, 161 (1964).
2. C. V. Shank, Rev. Mod. Phys., 47, 649 (1975).
3. J. P. Webb, Anal. Chem., 44, 30A (1972).
4. L. M. Fraser and J. D. Winefordner, Anal. Chem., 43, 1693 (1971).
5. M. B. Denton and H. V. Malmstadt, Appl. Phys. Lett., 18, 489 (1971).
6. L. M. Fraser and J. D. Winefordner, Anal. Chem., 44, 1444 (1972).
7. N. Omenetto, N. N. Hatch, L. M. Fraser and J. D. Winefordner, Spectrochim. Acta, 28B, 65 (1973).
8. N. Omenetto, N. N. Hatch, L. M. Fraser and J. D. Winefordner, Anal. Chem., 45, 195 (1973).
9. N. Omenetto, G. D. Boutelier, S. J. Weeks, B. W. Smith and J. D. Winefordner, Anal. Chem., submitted (1977).
10. N. Omenetto, P. Benetti, L. P. Hart, J. D. Winefordner and C. Th. J. Alkemade, Spectrochim. Acta, 28B, 289 (1973).
11. E. H. Piepmeier, Spectrochim. Acta, 27B, 431 (1972).
12. J. Kuhl, S. Neumann and M. Kriese, Z. Naturforsch., 28A, 273 (1973).
13. J. D. Winefordner, V. Svoboda and L. Cline, Crit. Rev. Anal. Chem., 1, 232 (1970).
14. N. Omenetto and J. D. Winefordner, "Atomic Fluorescence Spectroscopy with Laser Excitation," Chapter in Analytical Laser Spectroscopy, N. Omenetto, ed., Wiley-Interscience, New York, NY, in preparation.
15. D. K. Killinger, C. C. Wang and M. Hanabusa, Phys. Rev. A, 13, 2146 (1976).

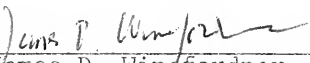
16. R. H. Pantell and H. E. Puthoff, Fundamentals of Quantum Electronics, Wiley, New York, NY (1969).
17. A. P. Thorn, Spectrophysics, Chapman and Hall, London (1974).
18. M. Hercher, Appl. Opt., 6, 947 (1967).
19. J. D. Winefordner, S. G. Schulman and T. C. O'Haver, Luminescence Spectrometry in Analytical Chemistry, Wiley-Interscience, New York, NY (1972).
20. A. C. G. Mitchel and M. W. Zemansky, Resonance Radiation and Excited Atoms, Cambridge Univ. Press, Cambridge, MA (1961).
21. H. P. Hoomayers, Ph. D. Thesis, Utrecht (1966).
22. W. L. Wiese, M. W. Smith and B. M. Miles, Atomic Transition Probabilities, Vol. II, Sodium through Calcium, U. S. Government Printing Office (1969).
23. J. J. Barrett and N. I. Adams III, J. Opt. Soc. Am., 58, 311 (1968).
24. H. Haraguchi and J. D. Winefordner, Appl. Spec., submitted (1977).
25. J. D. Winefordner, M. L. Parsons, J. M. Mansfield and W. J. McCarthy, Anal. Chem., 39, 436 (1967).
26. M. L. Parsons, B. W. Smith and G. E. Bentley, Handbook of Flame Spectroscopy, Plenum Press, New York, NY (1975).
27. J. D. Winefordner and T. J. Vickers, Anal. Chem., 36, 1947 (1964).
28. P. J. Th. Zeegers and W. P. Townsend, Spectrochim. Acta, 24B, 243 (1969).
29. P. Lijnse, Ph. D. Thesis, Utrecht (1973).
30. H. L. Brod and E. S. Yeung, Anal. Chem., 48, 344 (1976).
31. S. Neumann and M. Kriese, Spectrochim. Acta, 29B, 127 (1974).
32. W. M. Fairbank, T. W. Hänsch and A. L. Schawlow, J. Opt. Soc. Am., 65, 199 (1975).
33. B. W. Smith and M. L. Parsons, J. Chem. Ed., 50, 679 (1973).

34. C. H. Corliss and W. R. Bozman, Experimental Transition Probabilities for Spectral Lines of Seventy Elements, NBS Monograph 53, U. S. Government Printing Office (1962).
35. M. L. Parsons, B. W. Smith and P. M. McElfresh, Appl. Spec., 27, 471 (1973).

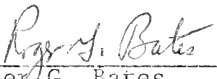
BIOGRAPHICAL SKETCH

Benjamin Willard Smith was born in Safford, Arizona, on May 10, 1951. He was graduated in June, 1969, from Safford High School in Safford, Arizona. In December, 1972, he received the Bachelor of Science Degree in Chemistry from Arizona State University in Tempe, Arizona. In January, 1972, he entered the University of Florida as a Graduate Student in the Department of Chemistry, College of Arts and Sciences.

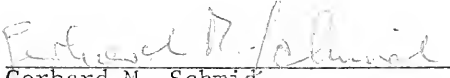
I certify that I have read this study and that in my opinion it conforms to acceptable standards of scholarly presentation and is fully adequate, in scope and quality, as a dissertation for the degree of Doctor of Philosophy.


James D. Winefordner, Chairman
Graduate Research Professor
of Chemistry

I certify that I have read this study and that in my opinion it conforms to acceptable standards of scholarly presentation and is fully adequate, in scope and quality, as a dissertation for the degree of Doctor of Philosophy.

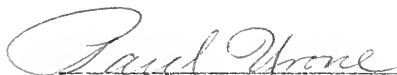

Roger G. Bates
Professor of Chemistry

I certify that I have read this study and that in my opinion it conforms to acceptable standards of scholarly presentation and is fully adequate, in scope and quality, as a dissertation for the degree of Doctor of Philosophy


Gerhard M. Schmid
Associate Professor of Chemistry

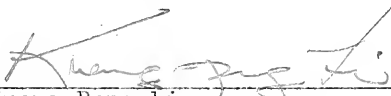


I certify that I have read this study and that in my opinion it conforms to acceptable standards of scholarly presentation and is fully adequate, in scope and quality, as a dissertation for the degree of Doctor of Philosophy.



Paul Urone
Professor of Environmental
Engineering

I certify that I have read this study and that in my opinion it conforms to acceptable standards of scholarly presentation and is fully adequate, in scope and quality, as a dissertation for the degree of Doctor of Philosophy.



Kuang-Pang Li
Assistant Professor of Chemistry

This dissertation was submitted to the Graduate Faculty of the Department of Chemistry in the College of Arts and Sciences and to the Graduate Council, and was accepted as partial fulfillment of the requirements for the degree of Doctor of Philosophy.

March 1977

Dean, Graduate School

Dec 1946 77 1452

MS